Tree Physiology 28, 1513–1523

Mechanical analysis of the strains generated by water tension in plant stems. Part II: strains in wood and bark and apparent compliance

TANCRÈDE ALMÉRAS[1]

[1] *INRA-UMR Ecofog, Campus Agronomique, BP 316, 97379, Kourou Cedex, French Guiana, France (t_almeras@hotmail.com)*

Received November 24, 2006; accepted May 5, 2008; published online August 1, 2008

Summary Tree stems shrink in diameter during the day and swell during the night in response to changes in water tension in the xylem. Stem shrinkage can easily be measured in a nondestructive way, to derive continuous information about tree water status. The relationship between the strain and the change in water tension can be evaluated by empirical calibrations, or can be related to the structure of the plant. A mechanical analysis was performed to make this relationship explicit. The stem is modeled as a cylinder made of multiple layers of tissues, including heartwood, sapwood, and inner and outer bark. The effect of changes in water tension on the apparent strain at the surface of a tissue is quantified as a function of parameters defining stem anatomy and the mechanical properties of the tissues. Various possible applications in the context of tree physiology are suggested.

Keywords: biomechanics, calibration, diurnal strains, mechanical model, multilayer cylinder, water potential.

Introduction

A tree stem contracts during the day because of an increase in water tension generated by transpirational flow, and expands during the night when the water tension decreases (Klepper et al. 1971, Zaerr 1971). These diurnal strains can easily be measured at the surface of the xylem, phloem or bark of a tree, e.g., with linear transducers (Klepper et al. 1971, Daudet et al. 2005) or strain gauges (Okuyama et al. 1995). Diurnal stem shrinkage and expansion have been taken into account to correct continuously recorded dendrometric data and to obtain unbiased information about cambial growth dynamics (Kozlowski and Winget 1964, Downes et al. 1999, Deslauriers et al. 2003). Because the developing cambial cells are subjected to this periodic mechanical stimulation (Okuyama et al. 1995, Abe and Nakai 1999, Yoshida et al. 2000*a*, Abe et al. 2001, Alméras et al. 2006*a*), diurnal stem diameter changes may directly affect wood morphogenesis. Variations in stem water potential can be monitored by continuous and nondestructive measurement of stem diameter changes providing a powerful tool for evaluating tree water status (Klepper et al. 1971, Simonneau et al. 1993, Panterne et al. 1998). A practical application of this method is in irrigation scheduling (Goldhammer and Fereres 2001, Remorini and Massai 2003). The method has also been used to study water transport (Parlange et al. 1975, Zweifel et al. 2000, Perämäki et al. 2001, Sevanto et al. 2002). Various derived applications have been proposed; for example, to evaluate the rate of embolism in a stem (Hölttä et al. 2002), the transport of sugar in phloem (Sevanto et al. 2003, Daudet et al. 2005) and the reduction in wood conductivity in senescent trees (Ueda and Shibata 2002).

The relationship between stem diameter changes and changes in stem water potential can be quantified empirically, by simultaneously recording changes in stem diameter and stem water potential (e.g., So et al. 1979) or from indirect measurements involving stem pressurization (Irvine and Grace 1997, Cochard et al. 2001, Alméras et al. 2006*b*). These calibration procedures are time-consuming, however, and the results for one plant material are not necessarily directly applicable to another, because the mechanical response to changes in water potential depends on the structure of the stem and its constitutive tissues, which vary among plants and may change with time. Various authors (So et al. 1979, Neher 1993, Irvine and Grace 1997) suggested that a mechanical analysis could help relate this calibration factor to the elastic properties of the plant tissues, which can be measured independently. Alméras and Gril (2007) presented a formulation of the mechanics associated with this question at the level of an individual cell and applied it to study the transmission of stress from water to the solid cell wall material. It was shown that the change in water pressure and the stress induced in the material are related by a parameter depending on tissue microstructure, termed the stress transmission factor (Alméras and Gril 2007). In the study reported here, this formulation has been used to compute the strain generated by the induced stress inside a stem. The complexity of stem anatomy is partly taken into account, to solve questions raised by previous experimental work: the contribution of wood and bark (here this term refers to all extra-cambial tissues) to the whole-stem strain (Ueda and Shibata 2001, Sevanto et al. 2003, Alméras et al. 2006*b*); the effect of an internal core of nonconducting tissues (Neher 1993, Irvine and Grace 1997, Ueda and Shibata 2002); the effect of outer bark (Neher 1993); and the computation of the relevant calibration factor. A comparison is made between the results of this study and previous approaches to the problem (So et al. 1979, Neher 1993, Irvine and Grace 1997). A general

formulation is kept, however, to allow application of the results to a wide range of plant material.

Parameters and use of the multi-layer cylinder model

A stem segment can be modeled as a multi-layer cylinder, with the formulation presented by Alméras and Gril (2007). In this model, each tissue is represented by a layer of homogeneous but anisotropic material. I will first analyze the behavior of a homogeneous cylinder to model the strains inside wood. Then, consideration of an inner core having different properties will provide a means to account for radial heterogeneity of wood stiffness, or for an internal layer of nonconducting tissue. Afterward, account is taken of the peripheral layers of bark by assuming they are much thinner than the wood. The inner bark (soft, living extra-cambial tissues, including phloem, but not limited to it) is assumed to be subjected to changes in water potential, whereas the dead outermost tissue of the bark is assumed to be separate from the water path, and thus unaffected by changes in water potential.

In wood, variations in osmotic potential π_w (see Table A1 in the Appendix for a list of symbols and their definitions) can be neglected, so that the change in stem water potential (Ψ_w) is equal to the change in hydrostatic pressure P_w ($\Psi_w = P_w + \pi_w \approx P_w$). In the inner bark, variations in osmotic potential π_b can be non-negligible. When diffusion equilibrium is achieved, the water potential is equal in the xylem and inner bark ($\Psi_w = \Psi_b = P_b + \pi_b$). Therefore, the change in hydrostatic pressure differs inside inner bark and wood ($P_b \approx P_w - \pi_b$). For simplification, the change in osmotic potential is ignored and the change in hydrostatic pressure is assumed uniformly equal to P.

In the model, the stem layers are numbered from inside to outside: subscript 0 refers to the center of the tree, 1 to the first wood layer, 2 to the second wood layer, 3 to the inner bark layer and 4 to the outer bark layer. The initial external radius of layer i is r_i. At equilibrium, its radial displacement is u_i and its radial stress is σ_i. The initial stress induced by the change in water pressure in layer i is assumed to be isotropic and equal to β_i. According to Alméras and Gril (2007), this parameter derives from the change in water pressure P and the stress transmission factor k_i:

$$\beta_i = -k_i P \tag{1}$$

Because a full cylinder is being considered, it is assumed that $r_0 = 0$ always. Even with this assumption, a hollow cylinder can be modeled by considering an innermost layer with null stiffness. The boundary condition at the internal radial bound is a full restraint in displacement ($u_0 = 0$). For a model with n layers, the boundary condition at the outer radial bound is free of stress ($\sigma_n = 0$). It is assumed that the stem strains freely in the longitudinal direction, and any variation of axial load is ignored, so that the longitudinal condition is $N = 0$ (Alméras and Gril 2007).

The problem is solved under these boundary conditions. Results will often focus on the field of tangential strain ε_T, because tangential strain is the "apparent" strain. The tangential strain $\varepsilon_{T,i}$ at the surface of layer i can be directly measured with strain gauges attached tangentially, or indirectly with a linear transducer recording the radial displacement u_i, and applying the formula:

$$\varepsilon_{T,i} = \frac{u_i}{r_i} \tag{2}$$

The mean radial strain $\varepsilon_{R,i}$ inside layer i can be computed from the radial displacements at its borders:

$$\varepsilon_{R,i} = \frac{u_i - u_{i-1}}{r_i - r_{i-1}} \tag{3}$$

The apparent compliance J_i at the surface of layer i, is defined as the ratio between the apparent strain and the change in water pressure (Alméras et al. 2006*b*):

$$J_i = \frac{\varepsilon_{T,i}}{P} \tag{4}$$

The inverse of this quantity, the apparent stiffness ($1/J_i$), is also considered to facilitate comparison with published results. Apparent compliance and stiffness, calculated from the tangential strain at the surface of a given layer, characterize the mechanical response of the whole structure, including inner layers.

The apparent compliance specific to a given layer, J'_i is computed based on the mean radial strain of this layer:

$$J'_i = \frac{\varepsilon_{R,i}}{P} \tag{5}$$

Equation 5 characterizes the specific mechanical response of the material of which the layer is made, independently of other layers.

Analysis of strains inside a homogeneous cylinder of wood

Parameter set for a standard hardwood

The reference set of parameters represents a standard water-saturated hardwood with a basic density of 650 kg m^{-3} (Guitard 1987). Elastic constants characterizing this material, and stiffness terms derived from it, are indicated in Table 1. The induced stress is set to an arbitrary tension of 1 MPa.

Fields of strain and stress

For a homogeneous cylinder composed of transverse isotropic material, and subjected to transverse isotropic induced stress, it is clear that, because no geometric incompatibility occurs, the strain fields are uniform and the residual stress field is null. However, if the material or the induced stress is anisotropic, the strain generated by the induced stress in a virtually isolated elementary volume of material is incompatible with the cylindrical geometry, so that heterogeneous fields of stress and

strain appear. The fields of radial displacement, and radial and tangential strains and stresses inside a cylinder of standard wood material were computed with the mechanical model described by Alméras and Gril (2007) and the above mentioned set of parameters and boundary conditions (Figures 1 and 2).

Radial displacement is negative and increases in magnitude from the center to the periphery of the wood. Radial and tangential strains are always negative (i.e., a contraction) because of the induced tension. Radial strain is lower than tangential strain because wood is stiffer in the radial direction. At the tree periphery, radial stress is null (i.e., in equilibrium with atmospheric pressure) and tangential stress is positive (i.e., the wood is under tangential tension). All strains and stresses decrease from the periphery to the center of the tree. Tangential stress becomes a compression near the center of the tree.

At first sight, the radial displacement appears approximately linear; but it is not. This is revealed by the derivative, the radial strain, which is subject to important variations. Irvine and Grace (1997) and Neher (1993) studied the field of displacement inside wood and found it approximately linear. This is consistent with our simulation results, and shows that this approximate linearity hides important heterogeneity in the strain and stress fields.

The field of tangential strains was simulated with sets of parameters modified from the reference hardwood. The values of E_R and E_T were modified to keep their product constant, but with various values of the E_R/E_T ratio (Figure 1C). The strain field is uniform if the material is transversely isotropic ($E_R/E_T = 1$). The heterogeneity of the tangential strain field and the magnitude of surface strains depend on the degree of transverse anisotropy of the material.

The tangential strain field was simulated by using various values of the Poisson's ratio ν_{RT}, keeping other parameters at their reference value (Figure 1D). Both the magnitude of peripheral tangential strain and their internal gradient are reduced by an increase in Poisson's ratio.

Simplified model neglecting longitudinal effects

Water tension also creates some longitudinal strain, resulting from two effects. The first is a contraction caused by the longitudinally induced stress, but it is low because of the large longitudinal stiffness of wood. The second is a small dilatation due to the coupling with the transverse contraction. The resulting strain is very low. In the simulation for the reference parameter set, the computed longitudinal strain is 6.7 μm m^{-1}. Yoshida et al. (2000*b*) also report that the longitudinal diurnal strain measured with strain gauges attached longitudinally is low and did not exceed 50 μm m^{-1} (M. Yoshida, personal communication). This value also includes the effect of variation in plant mass between day and night, especially bending

Table 1. Elastic constants, terms of the stiffness matrix and Poisson's ratios of the reference set of parameters representing a water-saturated hardwood with a density of 650 kg m^{-3} (from Guitard 1987). Abbreviations: E_R, E_T and E_L = radial, tangential and longitudinal modulus of elasticity, respectively; and C_{XY} = term X,Y of the stiffness matrix.

Elasticity (MPa)	Stiffness (MPa)	Poisson's ratios
E_R = 833	C_{RR} = 1,182	ν_{TL} = 0.033
E_T = 474	C_{TT} = 681	ν_{LR} = 0.386
E_L = 10,512	C_{LL} = 11,325	ν_{RT} = 0.675
	C_{TL} = 684	
	C_{LR} = 808	
	C_{RT} = 481	

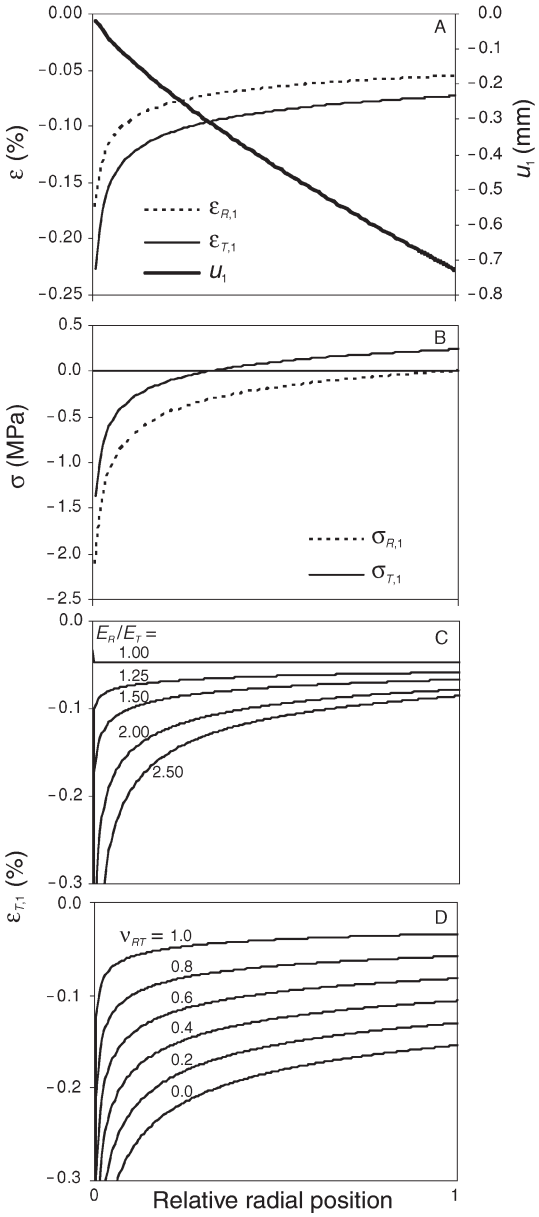

Figure 1. Radial fields of displacement, strain and stress caused by an induced tensile stress of 1 MPa inside a homogeneous cylinder of wood. Radial position is standardized by the stem radius (0 is the pith and 1 is the bark). (A) Fields of radial displacement (u) and radial and tangential strains (ε_R and ε_T, respectively). (B) Fields of radial ($\sigma_{R,1}$) and tangential ($\sigma_{T,1}$) stress. (C) Effect of wood anisotropy on the field of tangential strain: each line corresponds to a value of the E_R/E_T ratio. (D) Effect of the Poisson's ratio (ν_{RT}) of wood on the field of tangential strain: each line corresponds to a value of ν_{RT}.

effects, so that the strain resulting directly from the effect of water tension is probably less. In our simulation, tangential strain at the wood periphery was –0.073%. It becomes –0.078% if all longitudinal effects are neglected. This small change justifies neglecting these effects to further simplify the model.

Let us consider an orthotropic layer with internal radius r_{i-1} and external radius r_i, subjected to transverse isotropic induced stress β_i undergoing negligible longitudinal strain ($\varepsilon_L = 0$). Boundary conditions are an imposed displacement u_{i-1} at the internal bound and an imposed radial stress σ_i at the external radial bound of the layer. The mechanical problem can be explicitly solved, and, using the notation $\rho_i = r_{i-1}/r_i$, radial displacement at r_i is:

$$u_i = \frac{r_i(\sigma_i - \beta)\left(\rho_i^{-\gamma} - \rho_i^{\gamma}\right) + 2u_{i-1}\gamma C_{RR}}{C_{RT}\left(\rho_i^{-\gamma} - \rho_i^{\gamma}\right) + \gamma C_{RR}\left(\rho_i^{-\gamma} + \rho_i^{\gamma}\right)} \quad (6)$$

For a full cylinder comprising a single layer (denoted by subscript 1), this formula is applied with $\rho_1 = 0$, $u_0 = 0$ and $\sigma_1 = 0$. Use of this formula to compute the radial displacement leads to essentially the same results as in Figure 1 (0.725 mm instead of 0.729 mm at the tree periphery). From this expression, the apparent tangential strain at the periphery of a homogeneous wood cylinder is:

$$\varepsilon_{T,1} = \frac{u_1}{r_1} = \frac{-\beta}{C_{RT} + \gamma C_{RR}} \quad (7)$$

Apparent compliance of a full cylinder

Taking into account Equations 1, 4 and 7, the apparent compliance can be defined:

$$J_1 = \frac{\varepsilon_{T,1}}{P} = \frac{k}{C_{RT} + \gamma C_{RR}} \quad (8)$$

This parameter quantifies the linear relationship between water pressure and relative variations in wood diameter. It is emphasized that the apparent stiffness $1/J_1$ is equal to the radial modulus of elasticity (MOE) only for the special case of a transverse isotropic material having negligible Poisson's ratio and a stress transmission factor of 1. This can be appreciated easily if the apparent compliance is expressed as a function of the usual elastic constants:

$$J_1 = \frac{1}{E_R}\sqrt{\frac{E_R}{E_T}}\left(1 - \sqrt{\nu_{RT}\nu_{TR}}\right)k \quad (9)$$

where E_R and E_T are the radial and tangential MOE, ν_{RT} and ν_{TR} are the related Poisson's ratio (with $\nu_{TR} = \nu_{RT}E_T/E_R$). The difference between the apparent compliance and the inverse of the radial MOE is quantified by three corrective factors: the first refers to the effect of anisotropy; the second to Poisson's effect; and the third to the stress transmission between water and wood. For wood, the factor for anisotropy ranges between about 1.2 and 1.7, that for the Poisson's effect between 0.5 and 0.7, and that for the stress transmission factor between 0.5 and 0.9. The product of these factors ranges between 0.3 and 1, depending on wood structure and elastic properties. Based on data for water-saturated standard wood (Guitard 1987), the product of these factors yields 0.56 for a standard hardwood and 0.70 for a standard softwood. This means that wood typically appears about 1.5 to 2 times stiffer when subjected to internal pressure than when subjected to external load in its radial direction.

Based on a study of Monterey pines, Neher (1993) derived an empirical parameter and compared it with the measured radial MOE. For a stem of diameter (d) undergoing a change in wood diameter Δd when subjected to a change in pressure ΔP, he described the bulk modulus as:

$$K = \frac{\Delta P}{\frac{2\Delta d}{d}} \quad (10)$$

The bulk modulus theoretically expresses the relationship between a change in external isostatic pressure and the relative variation in the volume of a solid. Given that the relative variation in diameter is equal to the tangential strain, it is clear that $K = (1/J_1)/2$ according to Equation 8. Neher (1993) assumed that this quantity should be close to the radial MOE. Although the assumption is difficult to justify from a theoretical point-of-view, Neher (1993) found good agreement between the value of K determined experimentally by log pressurization (310 MPa) and the value of E_R determined by a bending test (320 MPa). It should be emphasized that the actual parameter of interest quantifying the link between apparent strain and pressure is the apparent stiffness $1/J_1 = 2K$, rather than the bulk modulus K. A reinterpretation of Neher's results suggests that the apparent stiffness $1/J_1$ is 620 MPa, i.e., about twice as large as the radial MOE. This is consistent with the numerical application of Equation 9, assuming that the product of corrective factors is equal to 0.5 for this wood.

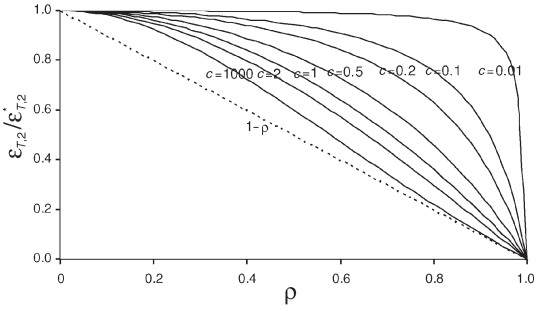

Figure 2. Reduction in apparent strain in response to an inner core of nonconducting tissue for various relative thicknesses of this core (ρ) and stiffness ratios (c).

Effects of heterogeneity of stiffness and induced stress

A simple model for two isotropic layers

The case of a homogeneous wood cylinder may be a limiting assumption when considering a stem with large radial variation in stiffness (e.g., ontogenetic variations in wood quality between juvenile and mature wood, or between heartwood and sapwood, or to model the effect of the pith or a hollow stem) or radial variation in induced stress (caused by a heterogeneous field of hydrostatic pressure, or heterogeneous stress transmission factor). In this case, a simple two-layer model allows the effect of heterogeneity to be quantified. The explicit resolution for a cylinder made of two thick orthotropic layers leads to an intractable formula. Therefore, to maintain an analytic approach, we consider a simpler case where the cylinder is made of two transverse isotropic layers, with moduli of elasticity C_1 and C_2, radii r_1 and r_2 and induced stress β_1 and β_2. With the notations $c = C_1/C_2$, $r = r_1/r_2$ and $b = \beta_1/\beta_2$, it can be shown (see Equation A1 in Appendix) that the surface strain is:

$$\varepsilon_{T,2} = \left(\frac{-\beta_2}{C_2}\right)\frac{2b\rho^2 + (1+c)(1-\rho^2)}{(1-\rho^2) + c(1+\rho^2)} \qquad (11)$$

Assuming a transverse isotropic material with negligible Poisson's ratio, this formula is correct for any thickness ratio. In the case of a general orthotropic material, parameters C_1 and C_2 can be approximated by $C_{RT,1} + \gamma_1 C_{RR,1}$ and $C_{RT,2} + \gamma_2 C_{RR,2}$, according to Equation 7. However, this approximation is good only if the internal layer is limited in radial extent. If the internal layer has both a preponderant contribution to the whole radius and important anisotropy, then the model with a thin external layer, shown in the next section, is more appropriate.

Internal layer of nonconducting tissues

Equation 11 can be used to compute the reduction in surface strain caused by an internal layer of nonconducting tissues. In this case, the stress induced in the internal layer is null ($\beta_1 = 0$, $b = 0$). The tangential strain that would be observed if there was no internal layer (i.e., if $r_1 = 0$, $\rho = 0$) is $\varepsilon^*_{T,2} = -\beta_2/C_2$. The ratio $\varepsilon_{T,2}/\varepsilon^*_{T,2}$ quantifies the reduction in surface strain caused by the nonconducting internal layer. It can be derived from Equation 11:

$$\frac{\varepsilon_{T,2}}{\varepsilon^*_{T,2}} = \frac{(1+c)(1-\rho^2)}{(1-\rho^2) + c(1+\rho^2)} \qquad (12)$$

This correction is plotted in Figure 2, for various values of c and ρ. If the inner layer has a low stiffness compared with the outer layer ($c \to 0$), for example, in the case of a pith or a hollow stem, the reduction in strain is negligible. The outer layer is not restrained by the inner layer, and can strain freely. In the opposite case ($c \to \infty$), the inner layer restrains the radial displacement at the interface with the outer layer, and therefore its tangential strain. Because of this restriction, some tangential stress appears that is necessarily balanced by additional radial strains. In the case of a large stiffness ratio, the strain reduction expressed by Equation 12 simplifies as $(1 - \rho^2)/(1 + \rho^2)$. For intermediate values of stiffness ratio, the outer layer is only partly restrained. If the difference in stiffness of the two layers is neglected (i.e., assuming $c = 1$), the strain reduction is $1 - \rho^2$, i.e., it is proportional to the surface area of the internal layer.

The field of tangential strain inside a stem made of two isotropic layers was computed for various sizes of the inner nonconducting layer (Figure 3). The ratio of tangential strain to the maximal tangential strain ε^*_T (which would occur at the periphery if there were no internal layer) is plotted against the relative radial position. Two cases are illustrated: a very stiff internal core ($c \to \infty$, Figure 3A) and negligible difference in stiffness ($c = 1$, Figure 3B). Tangential strain is always uniform in the inner layer, and increases inside the outer one. If the core is small, the gradient of tangential strain is steep near the core and decreases afterward. The larger the core, the more uniform the gradient becomes. If the core is very stiff, strains inside it are negligible. However, in the general case, strains appear in the core. These strains are caused not by a variation in internal water pressure (which we set to 0 inside the inner layer), but by the action of the outer layer. This likely explains the observations of Neher (1993), who found non-negligible strains in the heartwood of his tree No. 5, although he found no evidence of water conduction.

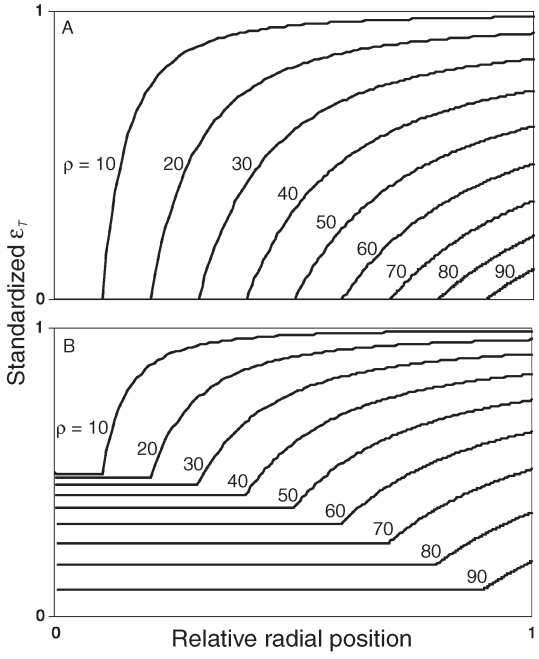

Figure 3. Effect of the relative thickness of a nonconducting core (ρ) on the radial field of tangential strains (ε_T). Strains are standardized by the maximal tangential strain, and radial positions by the external radius (0 is the pith and 1 is the bark). Each line depicts a different value of ρ (10, 20, 30, 40, 50, 60, 70, 80 and 90%). (A) Fields of ε_T obtained assuming that the core is much stiffer than the outer wood layer. (B) Fields of ε_T obtained when neglecting the difference in stiffness between the core and the outer layer.

To account for nonconducting tissues, Irvine and Grace (1997) based their computation on the estimated radial strain of sapwood, defined as the ratio between the radial displacement of wood and the thickness of sapwood. This is equivalent to assuming that the strain reduction factor is $1 - \rho$. This approximation is plotted in Figure 2. It is a good estimate only if the heartwood is much stiffer and thicker than the sapwood. Otherwise, this approximation always overestimates the reduction in strain. If it is not much stiffer than the sapwood, the heartwood also strains (Figure 3B), so that the radial strain of sapwood is incorrectly estimated by this approximation. If heartwood is not much larger than sapwood, strain concentration occurs near the core (Figures 3A and 3B), so that the mean radial strain of sapwood is not consistent with the reduction in strain caused by heartwood.

Apparent compliance of a cylinder with a nonconducting core

Neglecting the difference in stiffness between the internal and external layers, the apparent compliance for a 2-layer cylinder with nonconducting core is:

$$J_2 = \frac{\varepsilon_{T,2}}{P} = \frac{\left(1-\rho^2\right)\varepsilon^*_{T,2}}{P} \tag{13}$$

The specific apparent compliance of the wood material J'_2 was previously computed in the case of a homogeneous cylinder as J_1; therefore:

$$J'_2 = J_1 = \frac{\varepsilon^*_{T,2}}{P} \tag{14}$$

The relationship between the apparent compliance of the 2-layer cylinder J_2 and that of sapwood J'_2 can then be computed:

$$J_2 = \left(1-\rho^2\right)J'_2 \tag{15}$$

The apparent compliance of the 2-layer structure is lower than that of the sapwood, and the reduction factor is $1 - \rho^2$.

A study by Irvine and Grace (1997), followed by several later studies (Offenthaler et al. 2001, Perämäki et al. 2001, Hölttä et al. 2002), characterized the behavior of the sapwood by an apparent MOE defined as $E'_r = P/(\Delta r/r)$, where Δr is the change in radius and r is sapwood thickness. It can be expressed as a function of the apparent strain ε_T and the relative heartwood thickness ρ:

$$E'_r = \frac{P}{\varepsilon_T}(1-\rho) \tag{16}$$

The method of Irvine and Grace (1997) consists of two steps. First, the apparent modulus of sapwood is evaluated with Equation 16. Then, this property is assumed constant between trees, and a reversed form of Equation 16 is used to compute the pressure from the apparent strain in another stem, having a different sapwood thickness. However, because the factor used to account for sapwood thickness is biased, the apparent modulus of wood, E'_r, evaluated with this formula is generally not a property of the wood material independent of ρ. Its application to a stem with a different sapwood thickness may lead to biased results. It is correct only in two situations—if the relative thickness of sapwood is similar for the stems used for calibration and estimation, or if the stem used for calibration had a stiff and large heartwood. It is suggested that the apparent stiffness $1/J'$ is more appropriate than E'_r for characterizing the specific behavior of sapwood. It can be obtained from empirical data as (with Equations 13 and 15):

$$\frac{1}{J'} = \frac{P}{\varepsilon_T}\left(1-\rho^2\right) \tag{17}$$

The relationship between J' and elastic constants is given by Equation 9. The apparent compliance of a tree having different sapwood thickness can be computed with Equation 15.

For Norway spruce, Offenthaler et al. (2001) computed the apparent MOE based on simultaneous measurements of diurnal strains and changes in water potential, and found $E'_r = 830$ MPa. The heartwood accounted for about 75% of the wood diameter. With Equations 15, 16 and 17, the apparent stiffness of the sapwood and of the whole wood cylinder can be computed (Table 2). The two values differ greatly because of the important reduction in strain caused by the large heartwood core.

The mean value of E'_r calculated by Irvine and Grace (1997) was 750 MPa for Scots pine logs subjected to imposed pressure. In their study, the heartwood radius of the stems represented about 25% of the wood radius. Values of the deduced apparent stiffness of the sapwood and of the whole wood cylinder are indicated in Table 2. Note that the difference between these parameters is low in this case, which means that the effect of heartwood is practically negligible, because its radial extension is small. The prediction error could not be computed because sapwood thickness was not given for all trees studied by Irvine and Grace (1997). However, if the relative sapwood thickness is assumed constant between trees, predictions of water potential changes based on Equation 17 are 5 to 25% larger than those predicted by Irvine and Grace with Equation 16. The values derived with Equation 17 are closer to the actual water potentials measured by Irvine and Grace (1997).

Analysis of strains inside bark

A simple model with a thin outer layer

The inner bark can be modeled as a homogeneous layer with internal radius r_2 and external radius r_3 (with $\rho_3 = r_2/r_3$) submitted to transverse isotropic induced stress β_3. Because the internal cylinder of wood is much stiffer and thicker than the inner bark, it can be assumed that the effect of the inner bark on wood is negligible; i.e., that the radial displacement u_2 at the wood periphery calculated by the 2-layer model is approximately correct. Assuming that the radial stress at the periphery of inner bark σ_3 is known, the radial displacement u_3 at the sur-

face of the inner bark can be explicitly computed (see Equation A1 in Appendix). In the case of a thin layer ($1-\rho_3 \ll 1$), a first-order approximation of this expression is:

$$u_3 = \frac{r_3(\sigma_3-\beta_3)(1-\rho_3)}{C_{RR,3}} + u_2 \quad (18)$$

where $C_{RR,3}$ is the radial stiffness of inner bark.

Effect of outer bark

Let u_3^* denote the radial displacement in the case where the external radial stress is neglected (i.e., Equation 18 with $\sigma_3 = 0$). Let us assume that the inner bark is surrounded by a layer of outer bark, with internal radius r_3 and external radius r_4 (with $\rho_4 = r_3/r_4$), and which is not subjected to induced stress. This layer is deformed because of the displacement of the inner layer, u_3. As an elastic response to the deformation, the outer bark layer imposes a radial stress σ_3 at the interface with the inner bark. This stress will tend to restrain the radial displacement of the inner bark. Neglecting the Poisson's ratio of the outer bark and considering that $1-\rho_4 < 1$, a first-order approximation of this stress is:

$$\sigma_3 = -\frac{u_3}{r_3}(1-\rho_4)C_{TT,4} \quad (19)$$

where $C_{TT,4}$ is the tangential stiffness of outer bark. Combining Equations 18 and 19, the restraining effect of outer bark on inner bark can be quantified. It is expressed as a correction factor to apply to the radial displacement computed when the effect of outer bark is ignored:

$$u_3 = \frac{u_3^*}{1+\frac{C_{TT,4}}{C_{RR,3}}(1-\rho_3)(1-\rho_4)} \quad (20)$$

The correction factor is the product of the relative thickness of inner bark ($1-\rho_3$), outer bark ($1-\rho_4$) and the stiffness ratio of the bark layers $C_{TT,4}/C_{RR,3}$. A comparison with the results of the complete 4-layer model (Alméras and Gril 2007) was performed to validate and examine the full displacement field. It is plotted in Figure 4 for various postulated values of the bark stiffness ratio, for the case where inner and outer bark thickness are both equal to 5% of the wood radius. The graph shows that the radial displacement is significantly reduced only if outer bark is more than one order of magnitude stiffer than inner bark. It is apparent that the radial displacement of wood is reduced in the same proportion.

Few data are available on the transverse stiffness of inner and outer bark. Because these characteristics probably have large genetic, ontogenetic and environmental variabilities, it is difficult to assess the magnitude of this effect. We will assume that outer bark is no more than one order of magnitude stiffer than inner bark, and that both layers are thin, so that the compressive effect of outer bark can be neglected and Equation 18 can be used. This assumption differs from the experimental results of Neher (1993), who found a non-negligible restraining

Table 2. Apparent compliance (J) and apparent stiffness ($1/J$) of composite structures or single tissues calculated from published data. Abbreviations: Heart. = heartwood; Sap. = sapwood; and IB = inner bark.

Species	Tissue	J (% MPa^{-1})	$1/J$ (MPa)
Neher (1993)			
Monterey pine	Heart. + Sap.	0.16	620
	Phloem	16.6	6
Offenthaler et al. (2001)			
Norway spruce	Heart. + Sap.	0.030	3320
	Sap.	0.069	1453
Irvine et al. (1997)			
Scots pine	Heart. + Sap.	0.10	1000
	Sap.	0.11	940
Remorini et al. (2003)			
Peach tree	Whole stem	0.20	500
Klepper et al. (1971)			
Cotton	Whole stem	1.85	54.1
Molz and Klepper (1973)			
Cotton	Whole stem	2.96	33.8
	Xylem	0.36	280
	Bark	8.65	11.6
Ueda et al. (2001)			
Sugi	Wood + IB	0.10	969
	Wood	0.039	2560
Alméras et al. (2006b)			
Sugi	Wood + IB	0.11	926
	Wood	0.033	3049
	IB	0.70	143
Beech	Wood + IB	0.096	1163
	Wood	0.053	1898
	IB	0.61	163

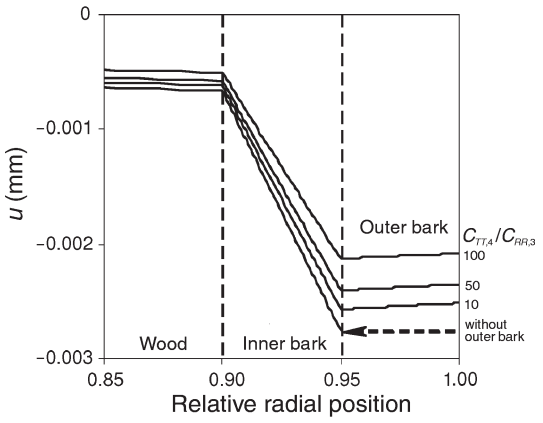

Figure 4. Field of radial displacement (u) at the tree periphery, computed for various values of the ratio of outer bark to inner bark stiffness $C_{TT,4}/C_{RR,3}$ = 10, 50 or 100.

effect of outer bark. Based on Equation 20, the outer bark should be almost three orders of magnitude stiffer than the phloem to be consistent with Neher's data on strain field and bark thickness. This high ratio cannot be excluded without independent data on bark stiffness, but these observations may partly result from measurement artifacts. For example, the effects of temperature variations (Lövdahl and Odin 1992) were corrected for based on a single value of the thermo-expansion coefficient of wood; however, this coefficient may differ greatly among inner and outer wood and bark. A larger coefficient in outer bark would possibly explain the results of Neher (1993). Hygro-expansion as a response to air humidity is also likely to be a non-negligible perturbation of the outer bark strain data (Lövdahl and Odin 1992). If such perturbations occur, it may be better to avoid interpreting outer bark data, and to concentrate on the interpretation of inner bark strains. Furthermore, because the outer bark is removed locally before measuring inner bark strains, it may be appropriate to neglect the outer bark effect when interpreting inner bark strain data.

Apparent compliance of wood and inner bark

The tangential strain on inner bark can be computed from Equation 18:

$$\varepsilon_{T,3} = \frac{u_3}{r_3} = (1-\rho_3)\varepsilon_{R,3} + \rho_3 \varepsilon_{T,2} \quad (21)$$

where $\varepsilon_{R,3} = -\beta_3 / C_{RR,3}$ is the mean radial strain in inner bark. The stress induced in inner bark is related to water pressure by the stress transmission factor $k_3 = -\beta_3 / P$. The apparent compliance at the surface of inner bark can be deduced as:

$$J_3 = \frac{\varepsilon_{T,3}}{P} = (1-\rho_3) J_3' + \rho_3 J_2 \quad (22)$$

where $J_3' = k_3 / C_{RR,3}$ is the apparent compliance of the inner bark tissue. The compliance of the whole structure results from contributions of the wood compliance and the inner bark compliance, weighted by their radial dimensions. The apparent compliance of the inner bark tissue can be expressed as a function of the usual engineering constants. The rigorous formula is provided in Equation A2 in the Appendix. In strongly oriented cellular solids, such as wood and phloem, $C_{RR} \approx E_R / (1 - \nu_{RT}\nu_{TR})$ is generally a good approximation. Therefore:

$$J_3' = \frac{k_3}{C_{RR,3}} \approx \frac{1}{E_R} k_3 (1 - \nu_{RT}\nu_{TR}) \quad (23)$$

As for the case of the wood cylinder (Equation 9), the apparent compliance of the inner bark material is not equal to the inverse of its radial MOE. Two corrective factors are involved. The first is the effect of stress transmission between the water and the cell wall. As shown by Alméras and Gril (2007), a reasonable estimate of this factor is 0.75 for wood. We will first assume the same value for inner bark. The second correction factor is the stiffening effect of the Poisson's ratio, because longitudinal and tangential strains are essentially restrained by kinematic conditions. Assuming that Poisson's ratios of inner bark are similar to those of the standard wood gives a value of 0.7 for this factor. The product of factors is then equal to 0.52, implying that inner bark is almost twice as stiff when subjected to internal pressure as when subjected to external radial tension. However, the precise quantification of these factors would require a more detailed analysis. Both the stress transmission factor and Poisson's ratio are likely to be highly affected by the specific structure of inner bark, and especially the presence of non-negligible numbers of non-vascular living cells and dead air-filled cells.

Contributions of wood and bark to apparent strains

Based on the formulae provided in this paper and experimental data, it is possible to compute the apparent compliance of composite stems or single tissues. The necessary data are the thickness of the stem tissues, and simultaneous measurements of strains and water potential in the field (Klepper et al. 1971, Ueda and Shibata 2001, Remorini and Masai 2003) or during rehydration (Molz and Klepper 1973) or pressurization experiments (Neher 1993, Alméras et al. 2006*b*). Table 2 presents values of apparent compliances obtained from various literature sources for which the necessary data were available. There is large variability in apparent compliances when composite stems are considered, and also in apparent compliance specific to a given tissue. This highlights the necessity of a reliable calibration method when working on a new material. Empirical calibration can be used together with the relationships with elastic properties and stem anatomy described in this article, to optimize predictions of changes in water potential from diurnal strain data.

The apparent compliance of wood ranges over one order of magnitude, from 0.03% MPa^{-1} for dense wood to 0.4% MPa^{-1} for the compliant xylem of a cotton stem (Table 2). The apparent compliance of inner bark is generally evaluated to be one or two orders of magnitude larger than wood, and ranges between 0.6 and 16% MPa^{-1}. The relative contributions of wood and bark to the strains at the tree surface depend on these compliance values, and also on relative bark thickness (cf. Equation 21). These parameters are shown in Table 3 for some published studies for which all data are available. The contribution of the wood to the apparent strain (i.e., the ratio between the tangential strain at the surface of wood and the tangential strain at the surface of the tree) ranges between 7.4 and 56.4%. In other studies for which the strains were reported at the surface of both tissues, the strain ratio lies within this range: 29% for a sapling of Japanese cedar submitted to artificial light–dark cycles (Alméras et al. 2006*b*), 31% for a Japanese cypress tree (Ueda and Shibata 2002) and 38% for a Scots pine under field conditions (Sevanto et al. 2002). The cases shown in Table 3 indicate that this ratio depends both on geometric effects (relative bark thickness) and on material effects (tissue compliance). The low contribution of wood to the strain in the cotton plant is due to its large relative bark thickness (34%).

The beech sapling has a larger wood contribution than the Japanese cedar mainly because of a difference in relative bark thickness (6% for the beech sapling versus 11% for the sugi sapling). The phloem of the Monterey pine is highly compliant compared with the other species, but this is compensated by its lower relative bark thickness (1.5%), so that the contribution of wood is intermediate.

Stem volume changes

Daily stem shrinkage and swelling implies a change in stem volume. The relative change in volume is equal to twice the tangential strain at the stem surface. If the daily amplitude in xylem water potential is 1 MPa, then the relative change in stem volume is equal to twice the apparent compliance of the stem. According to Table 2, it ranges between 0.2 and 6%. This volume change occurs in both xylem and bark. The contribution of wood to the relative change in volume is equal to the contribution of wood to the strains times the ratio of wood volume to stem volume. It ranges between 5 and 54% (Table 3).

Discussion

Contribution of wood and bark strain to plant water relations

The shrinkage and swelling of plant tissues have consequences on the hydraulic behavior of the plant. Variations in the amount of stored water result in a capacitance effect, buffering the changes in water flow and water potential. This effect has been taken into account in dynamic hydraulic models (e.g., Wronsky et al. 1985, Panterne et al. 1998, Génard et al. 2001, Perämäki et al. 2001, Zweifel et al. 2000, 2001). The contribution of stored water to transpiration flow directly depends on the stem capacitance parameter. In most studies, the value of this parameter is unknown and an adjusted value is used. Assuming that the change in stem water content is equal to its change in volume, capacitance can be related to the apparent compliance of the stem. For example, if the capacitance is defined by $C = \Delta Q/\Delta\Psi$, where ΔQ is the change in fractional water content and $\Delta\Psi$ the change in water potential (Panterne et al. 1998, Wronsky et al. 1985), then $C = 2J$, where J is the apparent compliance of the stem. The elastic properties of the tissues can therefore be used to feed capacitance parameters of dynamic sap flow models or validate the adjusted values.

Table 3. Contributions of wood and bark to the apparent strains and to the stem volume changes. Abbreviations: J = apparent compliance; ε = apparent strain; and ΔV = volume change.

Species	Tissue	J (% MPa^{-1})	Thickness (mm)	Contribution (%)	
				ε	ΔV
Neher 1993					
Monterey	Wood	0.16	132	38.9	38.4
pine	Phloem	16.6	2	61.1	61.6
Molz and Klepper 1973					
Cotton	Xylem	0.36	25	7.4	4.9
	Bark	8.65	13	92.6	95.1
Alméras et al. 2006b					
Sugi	Wood	0.033	2.92	25.3	23.9
	Inner bark	0.70	0.37	74.7	76.1
Beech	Wood	0.053	4.10	56.4	54.2
	Inner bark	0.61	0.26	43.6	45.8

The quantitative importance of the capacitance effect (i.e., its contribution to plant hydraulic regulation) is subject to discussion. Estimates of the stem volume change based on apparent compliances shown in Table 3 suggest that, if the tissues are compliant and the daily change in water potential is large, the change in stem volume can be several percent of the volume, i.e., the same order of magnitude as transpiration flow. These results are in agreement with those of Zweifel et al. (2001), and suggest that the mechanical properties and dimensions of stem tissues can have major consequences on plant water relations because they control the variations in stored water in response to changes in water potential.

In most of the above mentioned studies on dynamic sap flow models, strains in the xylem are considered negligible. Our result suggests that this is not generally true, because a large part of the stem volume change occurs in the wood compartment (Table 3), except for stems with a relatively thick bark. Wood is stiffer than bark tissues, but because its thickness is generally much greater, both tissues can make significant contributions to the strains and volume changes.

Potential applications of the model

There are various potential applications of diurnal strain data if independent estimates of the apparent compliance can be obtained. The most obvious is the nondestructive and continuous evaluation of variations in water potential. Some other possible applications in the field of tree physiology are briefly considered.

In inner bark, variations in osmotic potential have a non-negligible effect. In Equation 22, it was implicitly assumed that the variation in water pressure was the same in wood and inner bark. If variation in osmotic potential, π, occurs in inner bark at the same time as the variation in hydrostatic pressure, P, occurs in wood, then the apparent strain is:

$$\varepsilon_T(r_3) = (1-\rho_3)J_3'(P-\pi) + \rho_3 J_2 P \qquad (24)$$

The osmotic potential will reduce the apparent strain if P and π have the same sign, which is a usual situation (Sevanto et al. 2003). Equation 24 can therefore be used to evaluate the change in osmotic potential in inner bark of a stem by a nondestructive method, as suggested by Sevanto et al. (2003). If J_3' and J_2 can be evaluated independently, for example using the relationship with elastic properties, then the strain at the surface of wood can be used to evaluate P, and the strain at the surface of inner bark can be used to evaluate π.

Ueda and Shibata (2002) suggested that diurnal strains data could be used to evaluate the reduction in wood conductivity related to tree senescence. If the apparent compliance of sapwood can be evaluated independently, the diameter of non-

conducting tissues can be estimated with Equation 13.

Hölttä et al. (2002) performed a theoretical study on the relationship between xylem embolism and diurnal diameter changes. When cavitation occurs in a xylem conduit, the water tension is relieved so that the embolized conduit swells (i.e., recovers its unstressed state), and this has consequences for the xylem diameter as a whole. To account for it, Hölttä et al. (2002) consider an embolism rate defined as the surface area of embolized conduits divided by the total surface area. In the present formulation, this factor could be accounted for by considering that for a given water tension the induced stress is null inside a fraction of the xylem tissue equal to the embolism rate. It acts by reducing the macroscopic stress transmission by approximately this rate, and as a consequence, by reducing apparent compliance of the xylem. The embolism rate can then be evaluated from field data, by computing the reduction in wood compliance.

Acknowledgments

This study was supported by the grant-in-aid for scientific research no. 15.03742 from the Japanese Society for the Promotion of Science (JSPS). The author received a post-doctoral fellowship from the JSPS.

References

Abe, H. and T. Nakai. 1999. Effect of the water status within a tree on tracheid morphogenesis in *Cryptomeria japonica* D. Don. Trees 14:124–129.

Abe, H., T. Nakai, Y. Utsumi and A. Kagawa. 2001. Temporal water deficit and wood formation in *Cryptomeria japonica*. Tree Physiol. 23:859–863.

Alméras, T. and J. Gril. 2007. Mechanical analysis of the strains generated by water tension in plant stems. Part I: stress transmission from the water to the plant material at the cell level. Tree Physiol. 27:1505–1516

Alméras, T., M. Yoshida and T. Okuyama. 2006*a*. The generation of longitudinal maturation stress in wood is not dependent on diurnal changes in diameter of trunk. J. Wood Sci. 52:452–455.

Alméras, T., M. Yoshida and T. Okuyama. 2006*b*. Strains inside xylem and inner bark of a stem submitted to a change in hydrostatic pressure. Trees 20:460–467.

Cochard, H., S. Forestier and T. Améglio. 2001. A new validation of the Scholander pressure chamber technique based on stem diameter variations. J. Exp. Bot. 52:1361–1365.

Daudet, F.-A., T. Améglio, H. Cochard, O. Archilla and A. Lacointe. 2005. Experimental analysis of the role of water and carbon in tree stem diameter variations. J. Exp. Bot. 56:135–144.

Deslauriers, A., H. Morin, C. Urbinati and M. Carrer. 2003. Daily weather response of balsam fir (*Abies balsamea* (L.) Mill.) stem radius increment from dendrometer analysis in the boreal forests of Québec (Canada). Trees 17:477–484.

Downes, G., C. Beadle and D. Worledge. 1999. Daily stem growth patterns in irrigated *Eucalypus globulus* and *E. nitens* in relation to climate. Trees 14:102–111.

Génard M., S. Fishman, G. Vercambre, J.-G. Huguet, C. Bussi, J. Besset and R. Habib. 2001. A biophysical analysis of stem and root diameter variations in woody plants. Plant Physiol. 126: 188–202.

Goldhammer, D.A. and E. Fereres. 2001. Irrigation scheduling protocols using continuously recorded trunk diameter measurements. Irrig. Sci. 20:115–125.

Guitard, D. 1987. Mécanique du matériau bois et composites. Cepadues Edn., Toulouse, France, 238 p.

Hölttä, T., T. Vesala, M. Perämäki and E. Nikinmaa. 2002. Relationships between embolism, stem water tension and diameter changes. J. Theor. Biol. 215:23–38.

Irvine, J. and J. Grace. 1997. Continuous measurements of water tension in xylem of trees based on the elastic properties of wood. Planta 202:455–461.

Klepper, B., D.V. Browning and H.M. Taylor. 1971. Stem diameter in relation to plant water status. Plant Physiol. 48:683–685.

Kozlowski, T.T. and C.H. Winget. 1964. Diurnal and seasonal variations in radii of tree stems. Ecology 45:149–155.

Lövdahl, L. and H. Odin. 1992. Diurnal changes in the stem diameter of Norway spruce in relation to relative humidity and air temperature. Trees 6:245–251.

Molz, F.J. and B. Klepper. 1973. On the mechanism of water-stress-induced stem deformation. Agron. J. 65:304–306.

Neher, H.V. 1993. Effects of pressure inside Monterey pine trees. Trees 8:9–17.

Offenthaler, I., P. Hietz and H. Richter. 2001. Wood diameter indicates diurnal and long-term patterns of xylem water potential in Norway spruce. Trees 15:215–221.

Okuyama, T., M. Yoshida and H. Yamamoto. 1995. An estimation of turgor pressure change as one of the factors of growth stress generation in cell walls. Mokuzai Gakkaishi 41:1070–1078.

Panterne, P., J. Burger and P. Cruiziat. 1998. A model of the variation of water potential and diameter within a woody axis cross-section under transpiration conditions. Trees 12:293–301.

Parlange, J.-Y., N.C. Turner and P.E. Waggoner. 1975. Water uptake, diameter change and nonlinear diffusion in tree stems. Plant Physiol. 55:247–250.

Perämäki, M., E. Nikinmaa, S. Sevanto, H. Ilvesniemi, E. Siivola, P. Hari and T. Vesala. 2001. Tree stem diameter variations and transpiration in Scot pine: analysis using a dynamic sap flow model. Tree Physiol. 21:889–897.

Remorini, D. and R. Massai. 2003. Comparison of water status indicators for young peach trees. Irrig. Sci. 22:39–46.

Sevanto, S., T. Vesala, M. Perämäki and E. Nikinmaa. 2002. Time lags for xylem and stem diameter variations in a Scots pine tree. Plant Cell Environ. 25:1071–1077.

Sevanto, S., T. Vesala, M. Perämäki and E. Nikinmaa. 2003. Sugar transport together with environmental conditions controls time lags between xylem and stem diameter changes. Plant Cell Environ. 26:1257–1265.

Simonneau, T., R. Habib, J.P. Goutouly and J.G. Huguet. 1993. Diurnal changes in stem diameter depend upon variations in water content: direct evidence in peach trees. J. Exp. Bot. 44:615–621.

So, H.B., D.C. Reicosky and H.M. Taylor. 1979. Utility of stem diameter changes as predictors of plant canopy water potential. Agron. J. 71:707–713.

Ueda, M. and E. Shibata. 2001. Diurnal changes in branch diameter as indicator of water status of Hinoki cypress *Chamaecyparis obtusa*. Trees 15:315–318.

Ueda, M. and E. Shibata. 2002. Water status of Hinoki cypress (*Chamaecyparis obtusa*) under reduced hydraulic conductance estimated from diurnal changes in trunk diameter. Trees 16:523–528.

Yoshida, M., Y. Hosoo and T. Okuyama. 2000*a*. Periodicity as a factor in the generation of isotropic compressive growth stress between microfibrils in cell wall formation during a twenty-four hour period. Holzforschung 54:469–473.

Yoshida, M., O. Yamamoto and T. Okuyama. 2000*b*. Strain changes on the inner bark surface of an inclined coniferous sapling producing compression wood. Holzforschung 54:664–668.

Wronsky, E.B., Holmes, J.W. and N.C. Turner. 1985. Phase and amplitude relations between transpiration, water potential and stem shrinkage. Plant Cell Environ. 8:613–622

Zaerr, J.B., 1971. Moisture stress and stem diameter in young Douglas-fir. For. Sci. 17:466–469.

Zweifel, R., H. Item and R. Häsler. 2000. Stem radius changes and their relation to stored water in stems of young Norway spruce. Trees 15:50–57.

Zweifel, R., H. Item and R. Häsler. 2001. Link between diurnal stem radius changes and tree water relations. Tree Physiol. 21:869–877.

Appendix

Explicit field of radial displacement in a single layer

$$u_R(r) = \frac{r_1(\sigma_1 - \beta)\left(\left(\frac{r}{r_0}\right)^{\gamma} - \left(\frac{r}{r_0}\right)^{-\gamma}\right) - u_0 C_{RT}\left(\left(\frac{r}{r_1}\right)^{\gamma} - \left(\frac{r}{r_1}\right)^{-\gamma}\right) + u_0 \gamma C_{RR}\left(\left(\frac{r}{r_1}\right)^{\gamma} + \left(\frac{r}{r_1}\right)^{-\gamma}\right)}{-C_{RT}\left(\left(\frac{r_0}{r_1}\right)^{\gamma} - \left(\frac{r_0}{r_1}\right)^{-\gamma}\right) + \gamma C_{RR}\left(\left(\frac{r_0}{r_1}\right)^{\gamma} + \left(\frac{r_0}{r_1}\right)^{-\gamma}\right)} \quad \text{(A1)}$$

Relationship between the radial stiffness and elastic constants

$$C_{RR} = E_R \frac{1 - \nu_{TL}\nu_{LT}}{1 - 2\nu_{RT}\nu_{TL}\nu_{LR} - \nu_{TL}\nu_{LT} - \nu_{LR}\nu_{RL} - \nu_{RT}\nu_{TR}} \quad \text{(A2)}$$

Table A1. Symbols and their definitions.

Symbol	Definition
R, T, L	Radial, tangential and longitudinal directions, respectively
r_i	External radius of the ith layer
u_i	Radial displacement of the ith layer
u_3^*	Apparent radial displacement of inner bark in the absence of outer bark
$\varepsilon_{T,i}$	Tangential strain at the surface of the ith layer
$\varepsilon_{R,i}$	Mean radial strain inside the ith layer
$\varepsilon_{T,2}^*$	Apparent strain of sapwood in the absence of heartwood
σ_i	Radial stress of the ith layer
β_i	Isotropic stress induced in the ith layer
$C_{XY,i}$	Term X,Y of the stiffness matrix of the ith layer
C_1, C_2	Isotropic stiffness for the 2-layer model
γ_i	Anisotropy coefficient of the ith layer ($\gamma_i = \sqrt{C_{TT,i} / C_{RR,i}}$)
P	Change in hydrostatic pressure
π	Change in osmotic potential
Ψ	Change in water potential ($\Psi = P + \pi$)
ρ_i	Radius ratio of the ith layer ($\rho_i = r_{i-1}/r_i$)
k_i	Stress transmission factor of the ith layer
J_i	Apparent compliance at the surface of the ith layer
J_i'	Apparent compliance of the material of the ith layer
E_R, E_T, E_L	Directional components of the modulus of elasticity
E_r', Δr, r	Apparent modulus and related parameters defined by Irvine and Grace (1997)
K, ΔP, d, Δd	Bulk modulus and related parameters defined by Neher (1993)
ν_{RT}, ν_{TL}, ν_{LR}	Poisson's ratios
b, c	Induced stress and stiffness ratio, respectively, for the 2-layer model